


# Lipase maturation factor 1 affects redox homeostasis in the endoplasmic reticulum

Benjamin S Roberts<sup>1,†</sup>, Melissa A Babilonia-Rosa<sup>1,†</sup>, Lindsey J Broadwell<sup>2,‡</sup>, Ming Jing Wu<sup>1</sup> & Saskia B Neher<sup>1,\*</sup> 

## Abstract

Lipoprotein lipase (LPL) is a secreted lipase that clears triglycerides from the blood. Proper LPL folding and exit from the endoplasmic reticulum (ER) require lipase maturation factor 1 (LMF1), an ER-resident transmembrane protein, but the mechanism involved is unknown. We used proteomics to identify LMF1-binding partners necessary for LPL secretion in HEK293 cells and found these to include oxidoreductases and lectin chaperones, suggesting that LMF1 facilitates the formation of LPL's five disulfide bonds. In accordance with this role, we found that LPL aggregates in LMF1-deficient cells due to the formation of incorrect intermolecular disulfide bonds. Cells lacking LMF1 were hypersensitive to depletion of glutathione, but not DTT treatment, suggesting that LMF1 helps reduce the ER. Accordingly, we found that loss of LMF1 results in a more oxidized ER. Our data show that LMF1 has a broader role than simply folding lipases, and we identified fibronectin and the low-density lipoprotein receptor (LDLR) as novel LMF1 clients that contain multiple, non-sequential disulfide bonds. We conclude that LMF1 is needed for secretion of some ER client proteins that require reduction of non-native disulfides during their folding.

**Keywords** disulfide bonds; lipase maturation factor 1; lipoprotein lipase; protein folding; redox

**Subject Categories** Protein Biosynthesis & Quality Control

**DOI** 10.15252/embj.201797379 | Received 18 May 2017 | Revised 18 June 2018 | Accepted 20 June 2018 | Published online 1 August 2018

**The EMBO Journal (2018) 37: e97379**

## Introduction

Lipoprotein lipase (LPL) is a secreted, dimeric lipase that hydrolyzes triglycerides present in very low-density lipoproteins and chylomicrons. LPL is the enzyme primarily responsible for clearing triglycerides from the blood, and thus LPL deficiency results in severe hypertriglyceridemia (Hegele & Pollex, 2009). As a secreted protein, LPL transits the ER where its two N-linked glycans and five

intramolecular disulfide bonds are processed. LPL requires a specialized, ER-localized maturation factor, LMF1, for secretion (Peterfy *et al*, 2007). LMF1 was originally identified as the combined lipase deficiency (cld) mutation, a recessive mutation on mouse chromosome 17 resulting in lethal hyperchylomicronemia in neonatal mice (Paterniti *et al*, 1983). In humans and mice lacking LMF1, LPL misfolds and is thus not secreted to the plasma, resulting in a phenotype similar to LPL deficiency (Davis *et al*, 1990; Peterfy *et al*, 2007). LMF1 assists in the maturation of not only LPL but also the related, dimeric lipases endothelial lipase (EL) and hepatic lipase (HL; Paterniti *et al*, 1983; Ben-Zeev *et al*, 2011). Importantly, pancreatic lipase, (PL), a related, but monomeric lipase, does not require LMF1 (Briquet-Laugier *et al*, 1999). All four lipases have multiple disulfide bonds.

The mechanism by which LMF1 promotes dimeric lipase folding is not well understood. LMF1 is an ER-resident, 5-pass transmembrane protein that belongs to a superfamily of proteins with poorly characterized function (Doolittle *et al*, 2009). Intriguingly, LMF1 is expressed in tissues lacking dimeric lipases, suggesting it may assist in the folding of additional client proteins (Peterfy *et al*, 2007). We set out to understand the precise mechanism by which LMF1 promotes LPL maturation by identifying new LMF1-binding partners. Our proteomic and biochemical experiments show that LMF1 interacts with enzymes involved in N-linked glycosylation (UGGT1, UGGT2), the ER-resident oxidoreductases ERp72, ERp44, and ERdj5, and thioredoxin (TRX), a cytosolic protein that reduces disulfide bonds in other proteins. Each of these proteins proved to be important for LPL folding.

The oxidoreductases associated with LMF1 have known roles in the folding of large, oligomeric or otherwise challenging substrates. ERp72 is a protein disulfide isomerase (PDI) with narrow substrate specificity (Jessop *et al*, 2009b; Rutkevich *et al*, 2010). ERp72 specializes in processing proteins such as LPL that have multiple disulfide bonds and that are members of oligomeric complexes. ERdj5 is an ER-localized PDI family member that accelerates ER-associated degradation (ERAD) by reducing misfolded proteins and facilitates efficient protein folding by reducing non-native disulfides (Ushioda *et al*, 2008; Oka *et al*, 2013). ERp44 is important in thiol-mediated retention, a system in which monomers destined for

1 Department of Biochemistry and Biophysics, University of North Carolina at Chapel Hill, Chapel Hill, NC, USA

2 Department of Chemistry, University of North Carolina at Chapel Hill, Chapel Hill, NC, USA

\*Corresponding author. Tel: +919 966 9550; E-mail: neher@email.unc.edu

†These authors contributed equally to this work

‡Present address: Department of Biochemistry, University of Colorado at Boulder, Boulder, CO, USA

oligomeric complexes are retained in the ER until they are properly incorporated into higher order structures. ERp44 is also involved in the quality control of oligomeric proteins containing disulfide bonds (Hampe *et al*, 2015). Both ERp44 and ERdj5 need reducing equivalents to carry out their functions, but it is not known where these reducing equivalents come from.

We also found enzymes involved in N-linked glycosylation associated with LMF1: UGGT1 and its isoform UGGT2. N-linked glycosylation is closely tied to disulfide bond formation (Jessop *et al*, 2009a). UGGT1 acts after the initial processing of an N-linked oligosaccharide. If the glycoprotein has not achieved its native conformation, UGGT1 aids in folding by adding back a glucose residue, allowing another round of association with calnexin and calreticulin (Arnold *et al*, 2000). Finally, we found multiple oligomeric, secreted proteins rich in disulfide bonds associated with LMF1 and show that one such protein, fibronectin, is a new client protein that requires LMF1 for secretion.

## Results

To investigate the role of LMF1 in protein folding, we utilized proteomics to identify its novel-binding partners. LMF1 is a multi-pass, transmembrane protein and the harsh detergents needed to extract it from the membrane fraction disrupt its association with binding partners. We thus covalently linked LMF1 to its partners using either the reducible chemical crosslinker DSP or site-specific incorporation of the unnatural amino acid *p*-benzoylphenylalanine (*p*Bpa; Schematics in Fig 1A and B). *p*BPA is a photoreactive, cross-linkable amino acid that was co-translationally incorporated into LMF1 at an amber nonsense codon engineered into the protein by site-directed mutagenesis. LMF1 with integrated *p*BPA can be cross-linked to nearby proteins when UV light is applied to cells (Liu *et al*, 2007). For both methods, Western blots of purified LMF1-His and bound proteins showed multiple, higher molecular weight bands reacting with anti-His antibody (Fig 1C and D). Samples were resolved by SDS-PAGE, stained, and sample and control bands were excised, and then, proteins were analyzed by mass spectrometry (Fig 1E and F). A negative control for the *p*BPA experiment was generated by not including the *p*BPA. To generate a negative control for the DSP experiment, we did not induce LMF1 production with tetracycline.

Multiple proteins were identified with both crosslinking approaches. We sorted the identified proteins for subcellular compartment and spectral abundance in the experimental vs. control sample using Scaffold (Searle, 2010). Proteins residing in the ER enriched in the experimental sample are listed in Table 1. Importantly, one of these proteins, Sell1L, is a known LMF1-interacting protein (Sha *et al*, 2014). Another identified LMF1-interacting protein, calnexin, was previously shown to enhance LPL maturation and was downregulated when LMF1 was absent (Ben-Zeev *et al*, 2002; Zhang *et al*, 2003).

Overall, the list of ER-resident, LMF1-interacting partners was enriched in lectin chaperones and enzymes that process disulfide bonds. We selected several proteins (ERp72, PDI, ERp44, ERdj5, UGGT1, and UGGT2) in these two functional classes for further analysis. We tested the role of the novel LMF1-binding partners in LPL secretion. PL, which does not depend on LMF1 for

secretion, served as a control for global changes to the ER protein-folding environment. siRNAs against ERp72, PDI, ERp44, ERdj5, UGGT1, and UGGT2 were compared to a scrambled siRNA control. As shown in the media fraction of Fig 2A and B, knockdown of ERp72 decreased both PL and LPL secretion. Knockdown of ERp44, ERdj5, UGGT1, and UGGT2 decreased secretion of LPL much more dramatically than PL. Although the sequence of the siRNA used for UGGT1 was not present in UGGT2 and vice versa, we saw that levels of both proteins were reduced with either siRNA (Appendix Fig S1). Thus, LPL requires UGGT1 and/or UGGT2 for secretion. Knockdown of PDI increased secretion of LPL, potentially because PDI is known to mediate ER retention of other proteins (Ko & Kay, 2004). Loss of lipase secretion is quantified in Fig 2C. The efficiency of knockdown of each of the LMF1 interacting partners was measured in the lysate fraction (Fig 2A and B), and for most proteins, knockdown was similar for LPL and PL, as quantified in Fig 2D.

Because loss of several oxidoreductases affected LPL secretion, we looked for additional redox-active proteins in our mass spectrometry data. We found the cytosolic electron donor thioredoxin (TRX). Cytosolic proteins identified in our mass spectrometry experiments are listed in Appendix Table S1. We reduced cellular levels of TRX using siRNA and tested for effects on LPL and PL secretion. Decreases in cellular TRX levels dramatically reduced LPL secretion, but PL secretion was not affected (Fig 2E, media panel). Lipase secretion and TRX knockdown data are quantified in Fig 2C and D. We also tested LPL and PL secretion when TXNIP, a TRX inhibitor, was expressed from a plasmid. TXNIP binds reduced TRX through disulfide linkages and blocks its activity (Patwari *et al*, 2006). When increasing amounts of TXNIP plasmid was transfected into cells stably expressing each lipase, secretion of LPL, but not PL, was reduced (Fig 2F, media panel and TXNIP panel).

We next asked why decreased levels of a cytosolic reductase might affect LPL, but not PL secretion. A recent study showed that the cytosolic TRX system is needed for correct folding of ER client proteins that require disulfide editing (Poet *et al*, 2017). We therefore asked whether LPL has a special need for reduction in its disulfide bonds. A previous study suggested that LPL can form intermolecular disulfide-bonded aggregates in the ER, but the authors were unable to detect the aggregates (Ben-Zeev *et al*, 2002). We thus set out to determine whether LPL forms intermolecular disulfide bonds that would need to be reduced for the correct intramolecular disulfides to form. To do so, we compared LPL and PL produced in HEK293 cells by Western blotting. Samples were first resolved by SDS-PAGE under reducing or non-reducing conditions. To ensure that any large, disulfide-bonded aggregates transferred to the membrane for blotting, we soaked gels in a solution of 10 mM DTT prior to transfer. Only after this step, we were able to see large aggregates in the lysate and pellet fraction of LPL, but not PL, run under non-reducing conditions (Fig 3A, double and triple arrows). Because PL is soluble, it is not observed in the pellet fraction. LPL monomers, not aggregates, were observed in samples run with reducing loading dye (Fig 3A, monomer position is indicated by a single arrow). Thus, when produced in WT cells, LPL can be differentiated from PL by its formation of aggregates characterized by intermolecular disulfide bonds.

Because PL and LPL also differ in their requirement for LMF1, we next asked whether LPL aggregation was worse in the absence

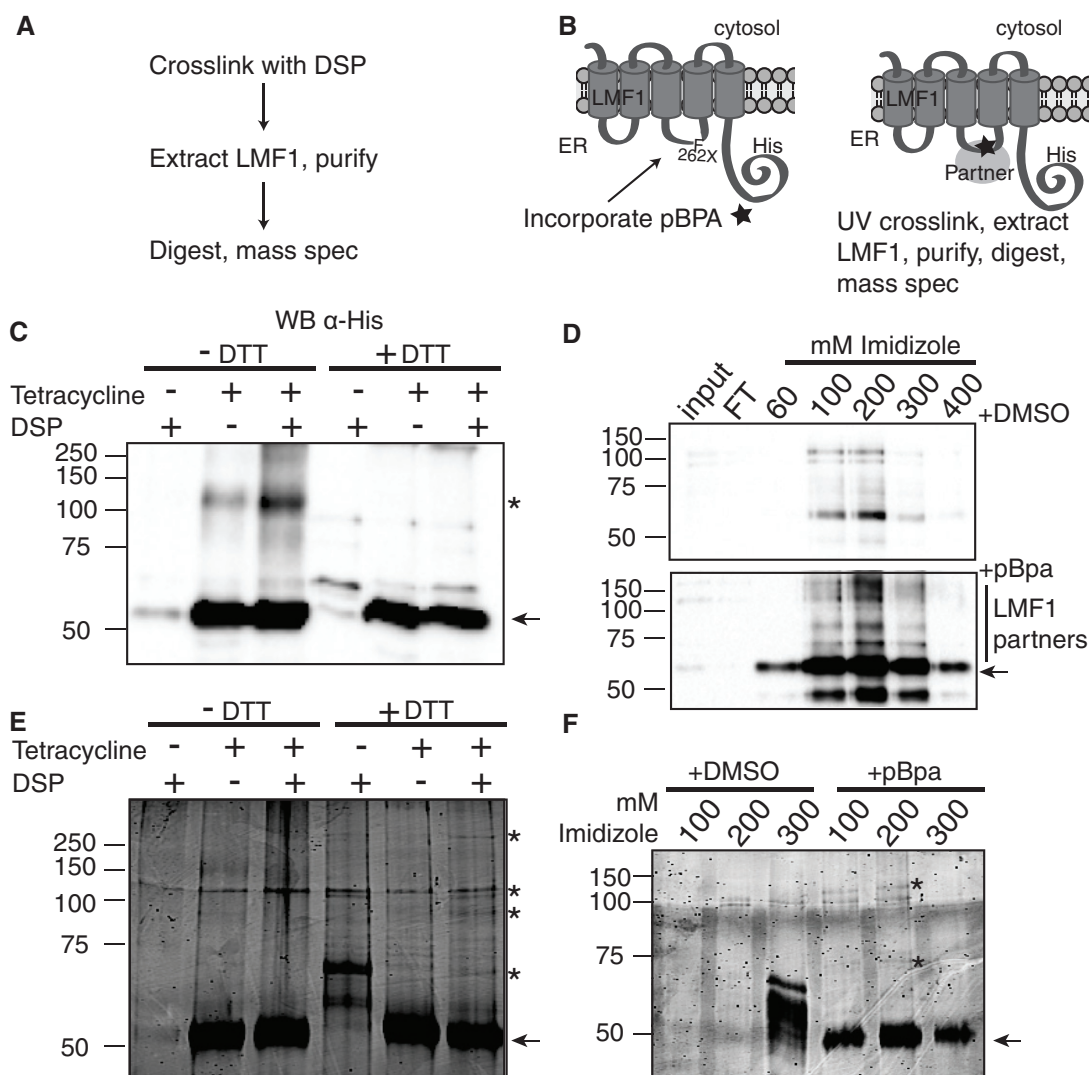


**Figure 1. Identification of new LMF1-interacting partners.**

**A** Experimental schematic of DSP crosslinking experiment.

**B** Schematic of pBPA crosslinking.

**C** Western blot of LMF1 partners after DSP crosslinking and affinity tag purification using LMF1's C-terminal His tag. Tetracycline induces LMF1 expression. Loading dye with 50 mM DTT was used to break the disulfide bonds between LMF1 and its interacting partners. LMF1 complexes are labeled with asterisks and an arrow points to LMF1.

**D** Western blot of LMF1 partners after pBPA photocrosslinking and affinity tag purification. The DMSO panel does not include pBPA and serves as a negative control. Fractions were eluted with increasing concentrations of imidazole. An arrow points to LMF1.

**E** SYPRO orange protein stain of DSP crosslinked samples. Samples without tetracycline but with DSP and DTT (negative control), and with tetracycline, DSP, and DTT were sent for LC-MS/MS. LMF1 complexes are labeled with asterisks and an arrow points to LMF1.

**F** SYPRO orange stained gel of pBPA samples. An arrow points to LMF1.

Source data are available online for this figure.

of LMF1. To carry out these tests, we used CRISPR/Cas to generate an LMF1 knockout in HEK293 Flp-In cells. We recovered a biallelic 22-base pair deletion in exon 1 of *LMF1* that results in a protein truncated at amino acid 27 (Appendix Fig S2). We refer to these cells as HEK293 $\Delta$ LMF1. We also have HEK293 Flp-In cells with a stably integrated, tetracycline-inducible copy of LMF1 (HEK293 + LMF1 cells). We compared LPL aggregation at steady state in HEK293 $\Delta$ LMF1, HEK293, and HEK293 + LMF1 cells by non-reducing

SDS-PAGE (Fig 3B). In HEK293 $\Delta$ LMF1 cells, very little monomeric LPL is seen in the lysate fraction (Fig 3B, single arrow), but the amount of soluble LPL increases when expression of LMF1 is driven from a strong promoter. The LPL absent from the lysate fraction in HEK293 $\Delta$ LMF1 cells is recovered in the pellet fraction, where large aggregates are observed (Fig 3B, double and triple arrows). As expected, there is less aggregated LPL in the pellet fraction of HEK293 and HEK293 + LMF1 cells.

**Table 1. ER-resident proteins with  $\geq$  peptides in the LMF1 sample than control sample from the DSP and/or pBPA crosslinking experiments.**

Protein	Symbol	MW, KDa	Sample	Sample peptides	Control peptides	Fold increase	P-value
Disulfide bond processing							
PDIA3	PDIA3_HUMAN	57	DSP/pBPA	12	4	1.5/INF	0.017
PDI	PDIA1_HUMAN	57	DSP/pBPA	11	2	1/INF	0.034
ERp72	PDIA4_HUMAN	73	DSP/pBPA	5	0	INF/INF	0.063
ERp44	ERP44_HUMAN	47	pBPA	2	0	INF	0.26
ERO1a	ERO1A_HUMAN	54	pBPA	2	0	INF	0.26
ERdj5	DJC10_HUMAN	91	DSP	3	3	1	0.45
PDIA6	PDIA6_HUMAN	48	DSP/pBPA	2	1	1/INF	0.51
Protein glycosylation/glycan processing							
Calnexin	CALX_HUMAN	68	DSP/pBPA	24	10	2.4/1	0.00042
UGGT1	UGGG1_HUMAN	177	DSP	2	0	2.8	0.00093
Alpha-glucosidase 2	GANAB_HUMAN	107	DSP	19	11	1.7	0.0077
MOGS	MOGS_HUMAN	92	DSP	17	6	2.3	0.053
Glucosidase II b	GLU2B_HUMAN	59	DSP/pBPA	5	0	INF/INF	0.063
Calreticulin	CALR_HUMAN	48	pBPA	4	0	INF	0.13
Ribophorin I	RPN1_HUMAN	69	DSP/pBPA	6	1	3/INF	0.13
UGGT2	UGGG2_HUMAN	175	DSP	2	1	INF	0.16
Exostosin-2	EXT2_HUMAN	82	DSP	1	0	INF	0.4
Chaperones							
Bip	GRP78_HUMAN	72	DSP/pBPA	45	17	2.9/3.3	0.0001
Endoplasmic	ENPL_HUMAN	92	DSP/pBPA	27	17	0.8/7	0.039
Cyclophilin B	PPIB_HUMAN	24	pBPA	5	0	INF	0.13
HYOU1	HYOU1_HUMAN	111	DSP	3	2	1.5	0.31
Metal binding							
SERCA2	AT2A2_HUMAN	115	DSP/pBPA	15	6	2/INF	0.019
E-Syt1	ESYT1_HUMAN	123	DSP	6	3	2	0.097
ZIP7	S39A7_HUMAN	50	DSP/pBPA	3	1	1/INF	0.26
STIM1	STIM1_HUMAN	77	DSP	1	0	INF	0.4
Reticulocalbin-2	RCN2_HUMAN	37	DSP	1	0	INF	0.4
Other enzymes							
P450R	NCPR_HUMAN	77	DSP	2	0	INF	0.16
ASP beta-hydroxylase	ASPH_HUMAN	86	DSP	1	0	INF	0.4
HACD3	HACD3_HUMAN	43	DSP	1	0	INF	0.4
Other ER-resident proteins							
LMF1	LMF1_HUMAN	65	DSP/pBPA	31	9	3.5/3.8	0.0012
SEC63	SEC63_HUMAN	88	DSP	15	8	1.9	0.012
Rab-1A	RAB1A_HUMAN	23	pBPA	2	0	INF	0.26
SEL1L	SE1L1_HUMAN	89	DSP	1	0	INF	0.4

Sample and control peptides are the total peptides from both experiments if the protein was identified in both samples. Fold increase for both experiments is listed. *P*-values are as reported from Scaffold, and if the protein was identified in both the DSP and the pBPA experiments, the lower value is listed.

In order to further analyze the effects of LMF1 on oxidative folding of LPL in the ER, we set up assays to analyze co-translational LPL folding in the presence of semipermeabilized (SP) cells (Francis *et al.*, 2002). In these assays, an *in vitro* translation system is charged with LPL mRNA to generate LPL protein

metabolically labeled with  $^{35}\text{S}$  methionine. Reactions were incubated in the presence of SP HEK293 or HEK293 $\Delta$ LMF1 cells in order to follow LPL maturation in the ER of these two cell types. Translation was stopped by the addition of cycloheximide and at the indicated time points, the thiol-modifying agent

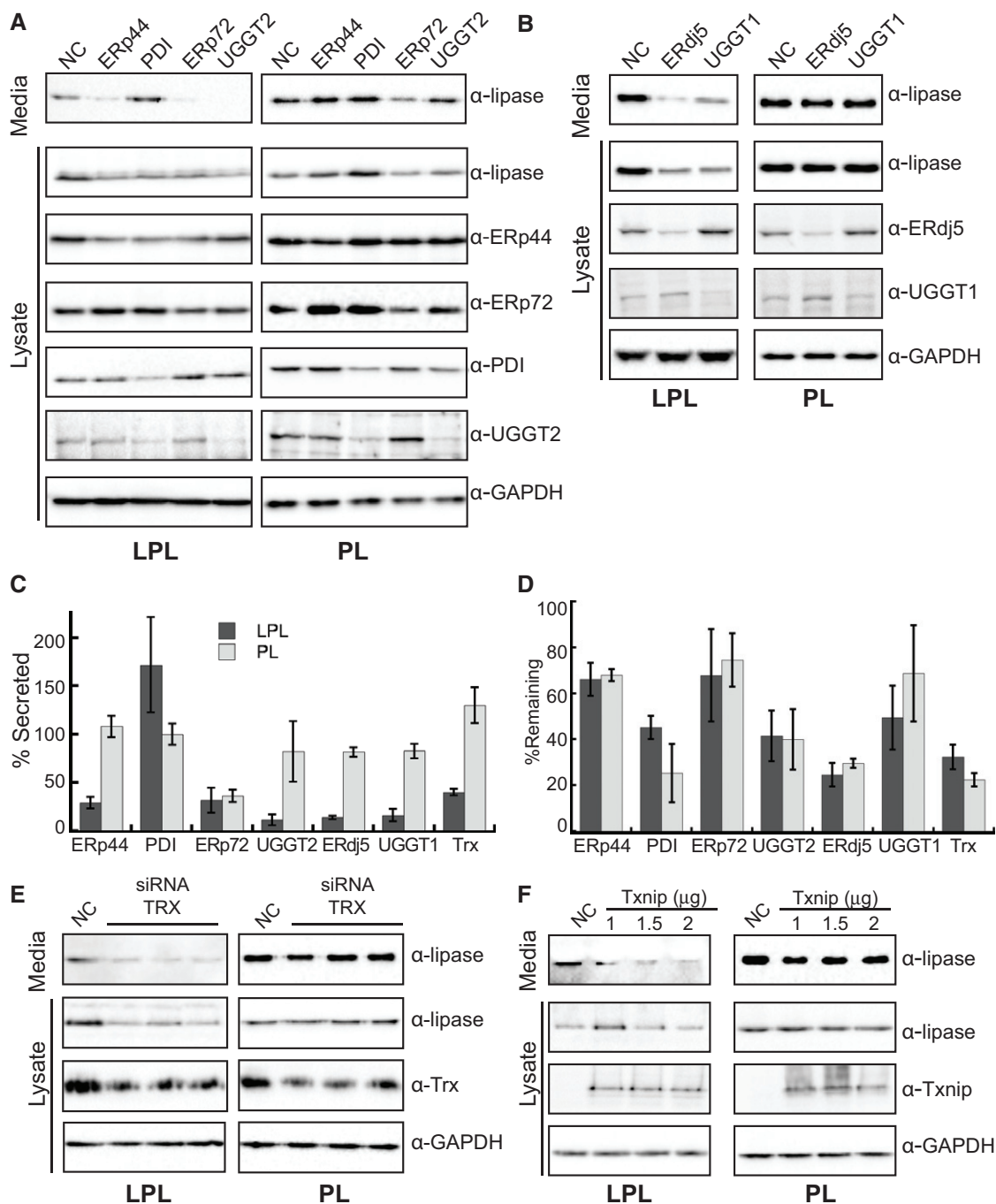


**Figure 2. siRNA knockdown of ERp44, ERp72, ERdj5, UGGT1, UGGT2, and TRX decreases LPL secretion.**

A, B HEK293 cells stably expressing LPL-V5 or PL-V5 were transfected with scrambled negative control siRNA (NC) or siRNA against LMF1-interacting partners. Media fractions were probed for the lipase V5 tags, and lysate fractions were probed for V5 and the LMF1-interacting partners. GAPDH is a loading control.

C siRNA knockdowns were performed in triplicate, and lipase secretion was quantified relative to NC siRNA. Error bars indicate the standard error.

D Quantification of the percent of each protein remaining from three independent experiments. Error bars indicate the standard error.

E HEK293 cells stably expressing LPL-V5 or PL-V5 were transfected with NC siRNA or siRNA against TRX. Lipase and TRX levels were tested as for Fig 1A.

F Txnip overexpression in HEK293 cells stably expressing LPL-V5 or PL-V5 hinders LPL, but not PL, secretion.

Source data are available online for this figure.

4-acetamido-4'-maleimidylstilbene-2,2'-disulfonic acid (AMS, which reacts with free cysteines in the protein increasing its molecular weight by 540 Da per AMS molecule) was added.

Samples were resolved by non-reducing SDS-PAGE and imaged. As shown in Fig 3C, and quantified in Fig 3D, LPL in HEK293 cells was initially more reduced, as indicated by a stronger upper,

AMS-modified band, as compared to LPL in HEK293ΔLMF1 cells. Furthermore, more LPL in the HEK293 cells than in the HEK293ΔLMF1 cells was chased to oxidized LPL over the 30-min timecourse (Fig 3C, quantified in Fig 3E). Finally, the HEK293ΔLMF1 cells showed a large and increasing band of aggregated, upper molecular weight LPL, whereas the HEK293 cells did not show as severe of aggregation (Fig 3C, quantified in Fig 3F). Figure 3G and H summarize LPL's oxidation state over time in HEK293 and HEK293ΔLMF1 cells, respectively.

We next tested how the loss of LMF1 affected cell survival after treatment with drugs [buthionine sulfoximine (BSO), dithiothreitol (DTT), and tunicamycin (Tm)] that perturb cellular redox homeostasis and protein folding. We carried out tests using HEK293 vs. HEK293ΔLMF1 cells and also carried out the tests in a line of immortalized mouse embryonic fibroblasts (MEFs) often used in the study of LMF1. These immortalized MEFs were either homozygous (*cld/cld*) or heterozygous (*cld/wt*) for the combined lipase deficiency (*cld*) mutation, which is a naturally occurring truncation mutation in *LMF1* resulting in loss of function (Paterniti *et al*, 1983; Briquet-Laugier *et al*, 1999; Peterfy *et al*, 2007).

We tested the sensitivity of cells to BSO because it lowers levels of glutathione by inhibiting its synthesis (Meister, 1983). Although glutathione is not required for protein folding in the ER (Tsunoda *et al*, 2014), we expected that cells lacking LMF1 would be more sensitive to BSO than wild-type cells if LMF1 contributes to reduction in the ER. Figure 4A and B shows that for both the HEK and MEF cell lines, cells lacking LMF1 were more sensitive to BSO relative to wild-type cells. Next, Tm blocks N-linked glycosylation, causing unfolded glycoproteins to accumulate in the ER, which induces the unfolded protein response (UPR). Many unfolded proteins are destined for ERAD. Prior to ERAD, disulfide bonds in disulfide-linked oligomers and unfolded monomers must be reduced, increasing the demand for ERdj5's reductase activity (Ushioda *et al*, 2008; Maegawa *et al*, 2017). If LMF1 contributes to reduction in the ER, cells lacking LMF1 should be hypersensitive to Tm. Figure 4A and B shows a trend of enhanced Tm sensitivity when cells lack LMF1. This difference was significant for the *cld/cld* vs. *cld/wt* MEFs (Fig 4B). Finally, DTT treatment also results in unfolded proteins and UPR upregulation, but because DTT reduces disulfides, cells with and without LMF1 should be equally sensitive to DTT if LMF1 contributes to reduction in the ER. Figure 4A and B shows that for both cell lines, the cells containing and lacking LMF1 were equally sensitive to DTT, indicating that misfolded proteins with reduced disulfides are not especially toxic to cells lacking LMF1.

To directly test the effect of loss of LMF1 on the redox environment in the ER, we used an ER redox probe. We tested HEK293ΔLMF1, HEK293, and HEK293 + LMF1 cells with the ER-targeted fluorescent redox sensor known as ERroGFP-S4 (Hoseki *et al*, 2016). ERroGFP-S4 has two redox-sensitive cysteines whose reduced and oxidized forms result in a protein with different excitation peaks (405 and 458 for oxidized and reduced, respectively). The ratio of fluorescence emission after excitation at each peak reports on the redox state of the ER. We used live cell fluorescence microscopy to compare HEK293, HEK293 + LMF1, and HEK293ΔLMF1 cells expressing ERroGFP-S4 alone or in combination with LPL-mCherry. Appendix Fig S3 shows ER-localized expression of ERroGFP-S4. As shown in Fig 4C, the fluorescence intensity ratio (Ex405/Ex458) was significantly higher for HEK293ΔLMF1 cells as compared to HEK293 and HEK293 + LMF1 cells, indicating a more oxidized ER. Expression of LPL-mCherry increased the oxidation of the ER in HEK293 cells, but again the fluorescence intensity ratio was significantly higher for HEK293ΔLMF1 cells. LMF1 thus contributes to maintaining the redox state of the ER, and its loss results in a more oxidized ER under normal and stress conditions.

How might LMF1 contribute to maintaining the redox state of the ER? Cysteine residues in proteins play key roles in diverse redox chemistry, and we therefore sought to better understand the nine cysteine residues in LMF1. We performed a BLAST alignment of the LMF1 protein sequence from multiple species and looked for conserved cysteines (Fig 5A and B). LMF1's nine cysteines showed strong overall conservation. However, in some species, cysteines 145, 188, and 288 were substituted for other residues. We mutated each cysteine and assessed LPL secretion. These experiments were done by transfecting wild-type or C-to-A mutant constructs into HEK293ΔLMF1 cells along with a plasmid expressing LPL-V5. Our early results revealed that mutation of C87 did not affect LPL secretion, and so we did not study it further. Figure 5C, media panel, shows that all other mutations reduced LPL secretion relative to WT LMF1. All of the mutant C-to-A LMF1 constructs expressed and could be seen in the pellet as expected for membrane proteins (Fig 5C, α-His pellet panel). Some mutants expressed better than others, but all expressed at higher levels than endogenous LMF1 (see Appendix Fig S4), which is present at such low levels that it is difficult to detect (Babilonia-Rosa & Neher, 2014). These data show that LMF1's cysteines are important for its ability to promote LPL secretion.

We next assessed LMF1's redox state. First, we resolved untreated LMF1 and LMF1 reduced with DTT by SDS-PAGE

### Figure 3. LPL forms disulfide-bonded aggregates when LMF1 is missing.

- A A Western blot against the C-terminal V5 tags of both lipases shows that LPL, but not PL, forms intermolecular disulfide bonds in cells. Lipase monomers are marked with a single arrow, and aggregates are marked with double and triple arrows. The LPL aggregates are not present when samples are treated with DTT. There is no PL in the pellet fraction because PL does not aggregate.
- B A Western blot of a non-reducing gel of the lysate and pellet fraction of LPL grown in cells lacking LMF1 (HEK293ΔLMF1), normal HEK293 cells, or cells with additional LMF1 (+LMF1). LPL monomers and aggregates are marked as above.
- C Co-translational LPL folding was carried out in the presence of SP HEK293 or HEK293ΔLMF1 cells. At the indicated time points, AMS was added to reactions to differentiate reduced (R) and oxidized (O) LPL. The position of the stacker layer is indicated.
- D–F The amount of reduced/total LPL intensity (D), the amount of oxidized/total LPL (E), and the intensity of the stacker/total LPL (F) were quantified. Each point is the average of three independent experiments, and error bars represent the standard deviation. Significance was determined by a two-tailed Student's *t*-test.
- G, H Data from (D–F) were combined to show the trends in LPL folding over time for reactions using HEK293 or HEK293ΔLMF1 cells. Each point is the average of three independent experiments, and error bars represent the standard deviation.

Source data are available online for this figure.

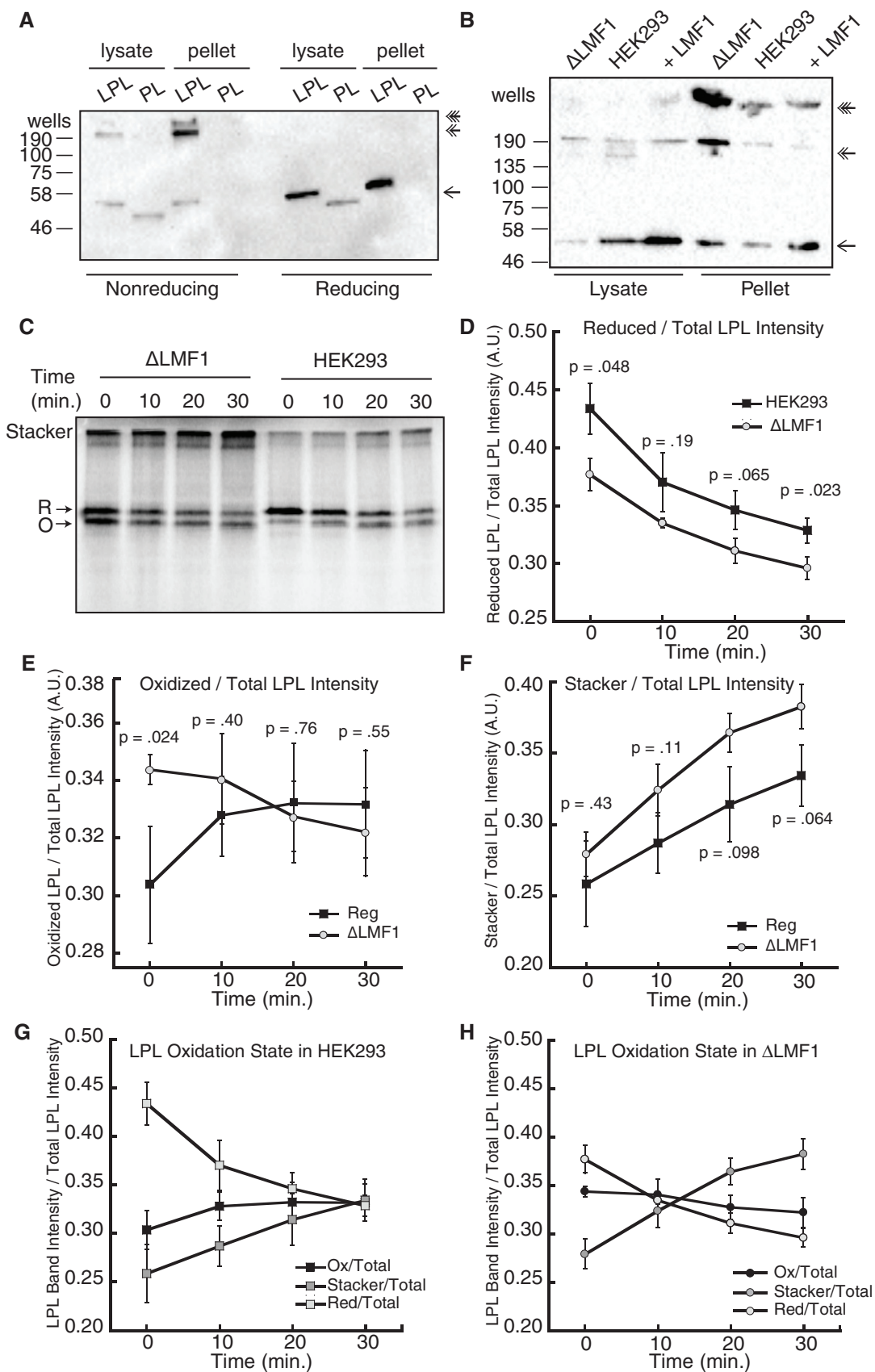
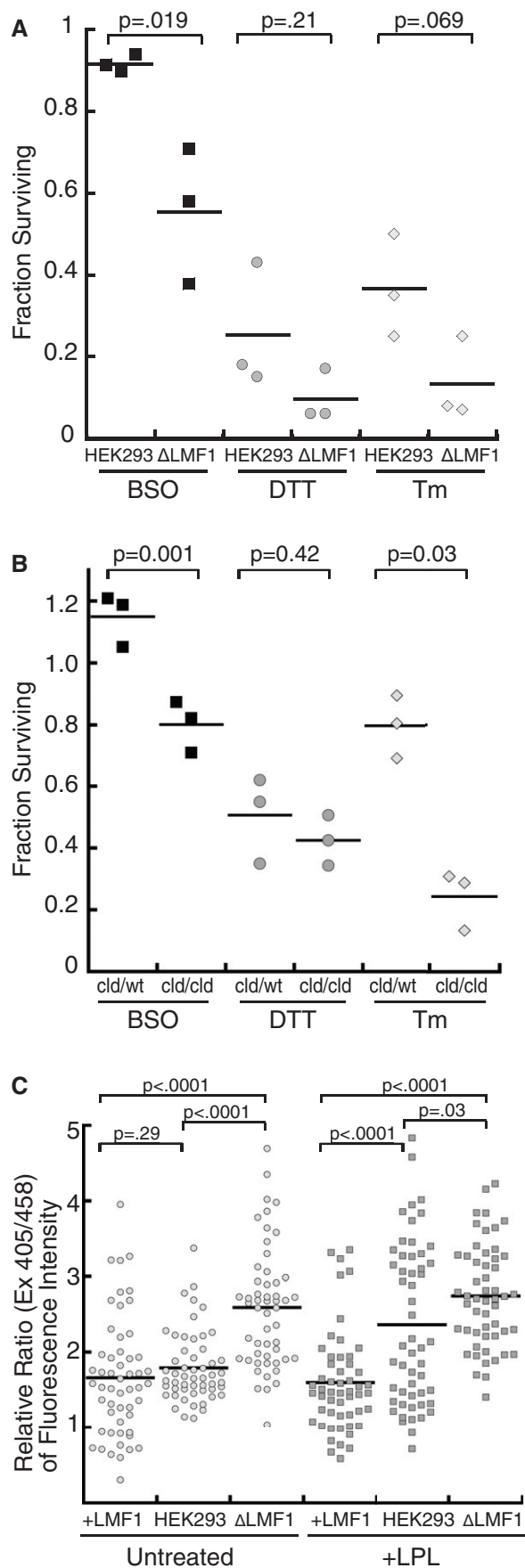


Figure 3.



**Figure 4. LMF1 contributes to redox homeostasis in the ER.**

A, B Differential sensitivity of HEK293 cells containing and lacking LMF1 (A) and *cld/cld* and *wt/cld* MEFs (B) to drugs that perturb cellular redox homeostasis. Cells were treated with BSO, DTT, or tunicamycin as described in Materials and Methods. Treated cell and untreated cells were counted, and the fraction of surviving cells was calculated. Three wells were counted and averaged for each data point, and three independent trials were carried out per condition. Significance was determined by a two-tailed Student's *t*-test.

C The redox sensor ERroGFP-S4 shows that HEK293 $\Delta$ LMF1 cells have a more oxidized ER than HEK293 and HEK293 + LMF1 cells both untreated and when stressed by expression of LPL-mCherry. A two-tailed Student's *t*-test was used to calculate the significance of the difference in the ratio of oxidized/reduced GFP fluorescence intensity between cell types. Each data point is one of three spots measured per cell, and 17 cells were measured per condition.

Source data are available online for this figure.

followed by Western blot (Fig 6A). These blots revealed that LMF1 runs slightly faster under non-reducing conditions, suggesting the presence of one or more disulfide bonds that compact its structure. However, when LMF1 was treated with AMS prior to SDS-PAGE resolution, its apparent molecular weight increased, indicating the presence of free cysteines. Pre-treatment with DTT prior to AMS treatment did not result in a sizable increase in LMF1's apparent molecular weight, indicating that the number of free cysteines likely outnumber the number of disulfide bonds. When hydrogen peroxide or a plasmid encoding TXNIP was added to cells expressing LMF1 prior to AMS treatment, we did not see a decrease in apparent molecular weight (indicating oxidation). Rather, we saw an increase in higher molecular weight aggregates, showing that LMF1 forms disulfide bonds with itself or other partners under these conditions.

To better understand the higher molecular weight species associated with LMF1, we acid trapped potential partners by using trichloroacetic acid (TCA) and blocking free thiols with NEM. LMF1 and associated proteins were then purified via LMF1's C-terminal His tag, and samples were visualized by Western blot against the His tag (Fig 6B). Some of the LMF1 was present in complexes larger than 190 kDa and in two distinct bands at approximately 90 and 120 kDa. Additionally, we saw an overall increase in His-reactive signal in this lane, indicating that LMF1 forms many interactions under non-reducing conditions. These high molecular weight signals were lost upon DTT treatment (Fig 6B +DTT panel). HEK293 $\Delta$ LMF1 cells were used as a negative control for cross-reacting bands (Fig 6B -LMF1 samples).

In addition to blotting for LMF1, we also blotted against two of the previously identified LMF1 partner proteins, ERdj5 and TRX. Using an antibody against TRX, we also found a band higher than the expected 12 kDa molecular weight of TRX in the LMF1 acid trap sample (at approximately 65 kDa), which was lost upon DTT treatment (Fig 6C). The active site of TRX is a CXXC motif, and replacing the resolving thiol with a hydroxyl group interrupts the oxidoreductase reaction resulting in generation of a "TRX trap" (Krupp *et al*, 2001). We found that co-expressing the TRX trap did not dramatically change the pattern of HIS-reacting bands (Appendix Fig S5A +TRX trap lanes). Furthermore, the TRX trap was Myc-tagged, and when we probed for the Myc tag, we did not see higher molecular weight Myc bands specific to the LMF1 trap samples (Appendix Fig S5B). However, there was a change in the pattern of Myc-reacting



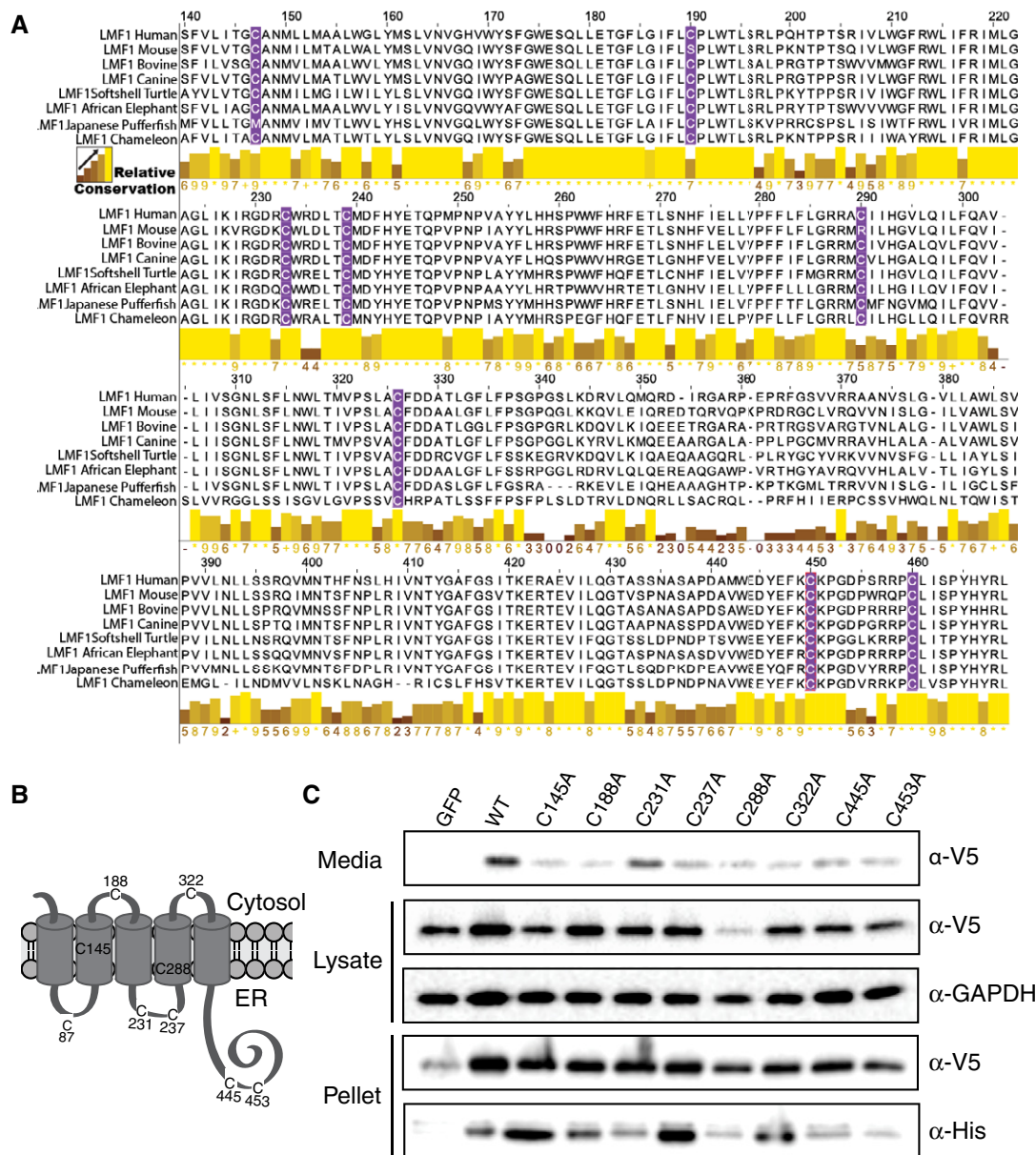


**Figure 5. Conserved cysteines in LMF1 are important to LPL secretion.**

A The LMF1 protein sequence from multiple species was aligned using Clustal Omega (Sievers *et al*, 2011).

B Schematic of the membrane topology of LMF1 showing the location of all the cysteines.

C Secretion of LPL-V5 from HEK293ΔLMF1 cells transiently transfected with LMF1 bearing the indicated cysteine to alanine mutations. Lipase levels in the lysate and pellet, and LMF1 levels in the pellet ( $\alpha$ -His), are also probed. GAPDH serves as a loading control.

Source data are available online for this figure.

bands in the load when LMF1 was present. We next co-expressed a V5-tagged version of ERdj5 and found a band higher (~135 kDa) than ERdj5's expected molecular weight of 91 kDa in the acid trap sample (Appendix Fig S5D). This band was lost upon addition of DTT. Thus, LMF1 has redox-active cysteines that appear to interact with TRX and ERdj5. However, both of these bands were faint, and neither band corresponds to the size of the major His-reacting bands in the LMF1 sample (Fig 6B). It is thus unclear that ERdj5 and TRX are LMF1's major partners.

Our results show that LMF1 plays a key role in oxidative protein folding, raising the question of whether it has other client proteins beyond dimeric lipases. To find additional LMF1 clients, we looked to our mass spectrometry results for secreted proteins associated with LMF1. We found fibronectin, a heavily disulfide-bonded, dimeric component of the extracellular matrix. We compared secretion of a fluorescently tagged variant of fibronectin in *clt/wt* and *clt/clt* cells. By confocal microscopy, a defect in fibronectin trafficking was apparent in *clt/clt* cells. As expected,

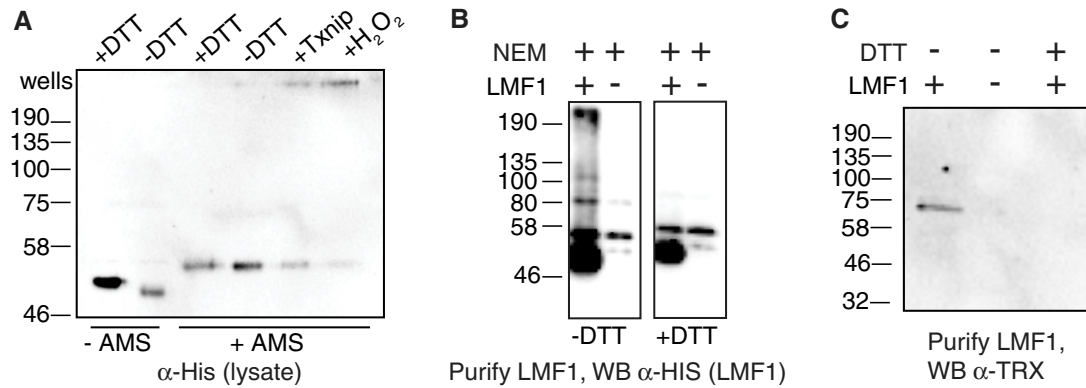


**Figure 6. Analysis of LMF1's redox-dependent interactions.**

**A** α-His Western blot to detect the redox state of LMF1. In the first two lanes, samples were untreated and resolved in reducing or non-reducing loading dye. The next four lanes were subject to the indicated treatments prior to cell lysis then treated with AMS prior to non-reducing SDS-PAGE.

**B** α-His Western blot to detect acid trapped partners of LMF1. Samples were TCA precipitated, treated with NEM, and LMF1 was purified via its C-terminal His tag. Samples were resolved by reducing or non-reducing SDS-PAGE. The lanes marked -LMF1 are HEK293ΔLMF1 cells included as a negative control.

**C** Samples were prepared as in (B), but were probed with an antibody for TRX.

Source data are available online for this figure.

fibronectin localized to the ER and cell surface in *clt/wt* cells. For the *clt/wt* cells in Fig 7A, fibrils containing fibronectin can be seen at the top, periphery, and bottom of each cell. However, in *clt/clt* cells, fibronectin was co-localized with the ER marker mCherry-Sec61β and was less apparent in the fibrils on top, bottom, and periphery of the cells (Fig 7A, quantified in Fig 7B). We confirmed that LMF1 is able to rescue the defect in fibronectin secretion of the *clt/clt* cells as the fibrils are restored when a plasmid expressing LMF1 is present (Appendix Fig S6A). Fibronectin secretion is also compromised in the HEK293ΔLMF1 cells (Appendix Fig S6B), but the defect is most evident in the *clt/clt* cells because, as MEFs, the cells secrete large quantities of extracellular matrix. Fibronectin is thus LMF1's first non-lipase client protein, and it shares structural characteristics including N-linked glycans, disulfide bonds, and oligomeric state with LMF1's known lipase substrates. Fibronectin was trapped as a mixed disulfide client of ERdj5, suggesting that LMF1 could act on fibronectin through ERdj5 (Oka *et al*, 2013).

To determine whether other ERdj5 clients depend on LMF1 for secretion, we tested the localization of GFP-tagged low-density lipoprotein receptor (LDLR) in HEK293, HEK293 + LMF1, and HEK293ΔLMF1 cells. LDLR is a large, multidomain protein with 30 disulfide bonds. LDLR folds non-vectorially, with non-native disulfide bonds between cysteines of different domains forming during on-pathway steps in folding (Jansens *et al*, 2002). ERdj5 later reduces these non-native disulfides so that the native disulfides can form (Oka *et al*, 2013). We did not find LDLR in our mass spectrometry results (LDLR is not expressed to high levels in kidney cells) but hypothesized that if LMF1 interacts with ERdj5 and ERdj5 acts on LDLR, then HEK293ΔLMF1 cells will be defective in secretion of LDLR. As shown in Fig 7C, and quantified in Fig 7D, LDLR is visible mainly at the plasma membrane in HEK293 + LMF1 and HEK293 cells. However, in HEK293ΔLMF1 cells, LDLR secretion is impaired and much of the LDLR is contained within the ER. Although this LDLR is within the confines of the ER, it appears punctate and

separate from the bulk of the ER, likely indicating severe aggregation. This is most evident in Movies EV1–EV3, which show a 3D reconstruction of the three cell types. Thus, LDLR, a known ERdj5 client, also requires LMF1.

## Discussion

LMF1 was initially identified as the *clt* mutation in mice, which resulted in deficiency of both LPL and HL activity such that affected mice died of hyperchylomicronemia shortly after birth (Paterniti *et al*, 1983). The *clt* mutation was later mapped to an ER-resident, transmembrane protein and named LMF1, but the precise mechanism by which it aided in dimeric lipase folding remained a mystery until now (Peterfy *et al*, 2007). Here, we show that LMF1 does more than just assist in the maturation of dimeric lipases. It is key to the secretion of at least two additional proteins, fibronectin and LDLR. What do LPL, HL, EL, fibronectin, and LDLR have in common? All three lipases are dimers whose monomers contain N-linked glycans and multiple intramolecular disulfide bonds. Our data show that LPL forms inappropriate intermolecular disulfide bonds (Fig 3). LPL thus has a special need for reduction in mispaired intermolecular disulfide bonds that PL, as a monomer, does not form. Fibronectin is an oligomer that contains seven N-linked glycans and 28 mostly non-consecutive intramolecular disulfide bonds. Fibronectin also forms two intermolecular disulfide bonds, a process that occurs most efficiently in cells (Vartio & Kuusela, 1991). The oxidoreductases needed for efficient fibronectin folding are not known, but trapping experiments indicate that fibronectin is an ERdj5 client (Oka *et al*, 2013). LDLR contains five N-linked glycans and 30 mostly non-consecutive intramolecular disulfide bonds. As a part of its folding pathway, LDLR forms non-native disulfides (Jansens *et al*, 2002). ERdj5 later reduces these disulfides so that the native bonds can be formed (Oka *et al*, 2013). LPL, fibronectin, and LDLR thus all have different challenges to the formation of the

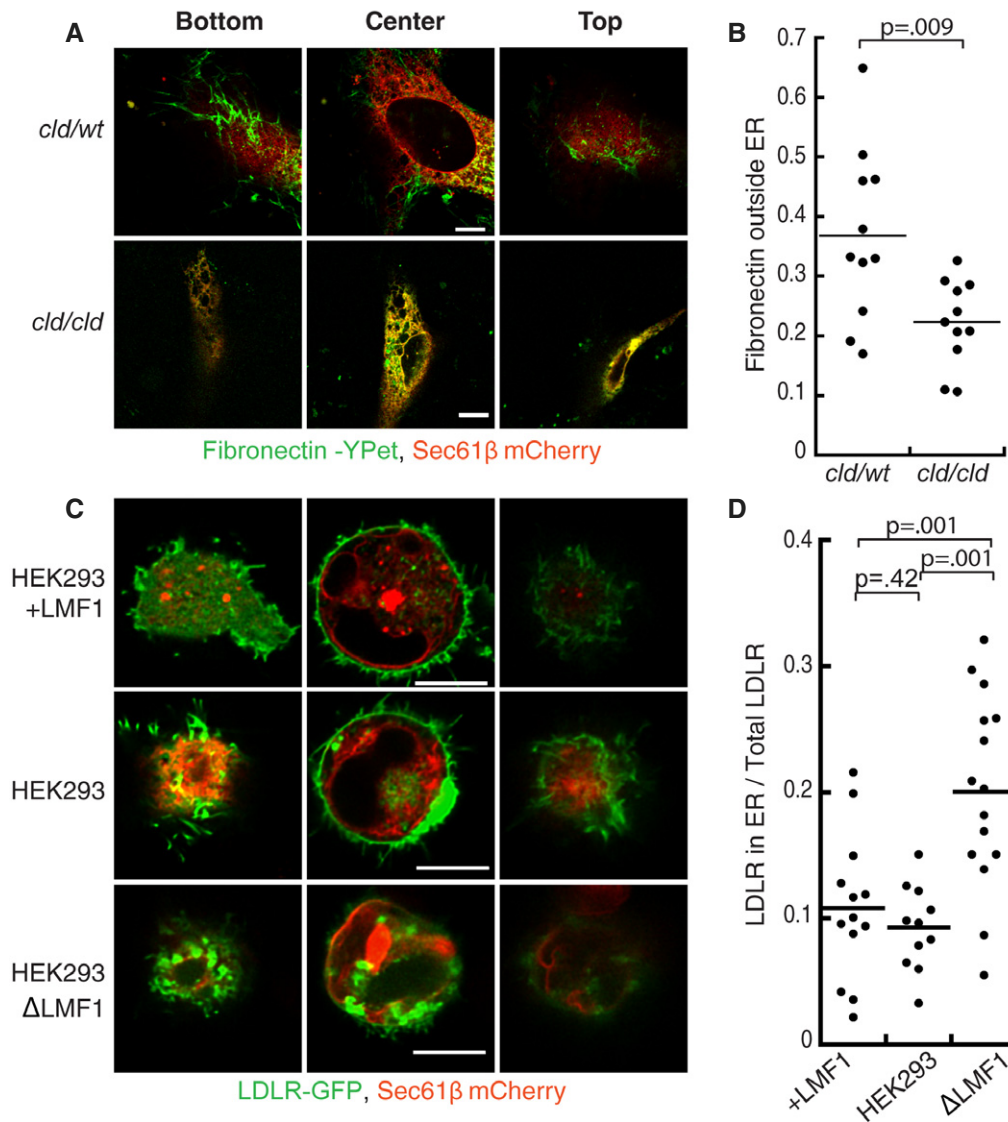


**Figure 7. Fibronectin and LDLR depend on LMF1 for secretion.**

A Bottom, center, and top slices from a z-stack of a *cld/wt* or *cld/cld* MEF cell. YPet-tagged fibronectin is in green, and mCherry-Sec61 $\beta$ , an ER marker, is in red. Note fibronectin assembly into the extracellular matrix in *cld/wt* cells.

B *cld/wt* cells had significantly higher amounts of fibronectin outside of the ER than *cld/cld* cells by a two-tailed Student's *t*-test.

C Bottom, center, and top slices show that LDLR is retained in the ER in cells HEK293 $\Delta$ LMF1 cells. LDLR-GFP is in green, and mCherry-Sec61 $\beta$  is in red. Note the clumping of LDLR in the ER in HEK293 $\Delta$ LMF1 cells.

D The ratio of LDLR within the ER/total LDLR was significantly higher for HEK293 $\Delta$ LMF1 cells than HEK293 or HEK293 + LMF1 cells by a two-tailed Student's *t*-test.

Data information: For all panels > 10 cells were measured per genotype. All scale bars are 10  $\mu$ m.

Source data are available online for this figure.

correct disulfide bonds, but these challenges are unified in that they can be overcome by disulfide reduction and re-shuffling.

How might LMF1 assist in the folding of these five substrates? We find that loss of LMF1 results in a more oxidized ER, suggesting that LMF1 contributes, directly or indirectly, to the reduction of the ER (Fig 4C). This role for LMF1 is consistent with its substrates' need for reductive disulfide shuffling. A recent, excellent review outlines four mechanisms for transferring reducing equivalents from the cytosol to the ER: (i) entry of cysteine thiols contained in nascent

proteins, (ii) import of reduced glutathione, (iii) transfer of reducing equivalents from the cytosolic thioredoxin system via an unidentified membrane protein, and (iv) action of an unknown, NADPH-dependent, ER-localized reductase (Ponsero *et al*, 2017; Ellgaard *et al*, 2018). Based on our microscopy results, it is clear that loss of LMF1 does not prevent entry of client proteins into the ER, indicating that the first mechanism is not involved. Next, LDLR maturation is independent of ER glutathione levels, but dependent on LMF1, making the second mechanism unlikely (Tsunoda *et al*, 2014).

Below, we speculate on a role for LMF1 in one of the remaining two possible mechanisms.

Interest in an unidentified eukaryotic transmembrane electron transporter comes from comparison to bacteria, where the periplasmic protein DsbC reduces misoxidized proteins in order to shuffle their disulfide bonds (Rietsch *et al*, 1997; Berkmen *et al*, 2005). The transmembrane electron transporter, DsbD, then catalyzes the transfer of electrons from the cytosolic donor, TRX, to recycle DsbC back to the reduced state (Rietsch *et al*, 1997). DsbD passes electrons using conserved cysteines that participate in a cascade of disulfide bond formation and reduction steps (Stewart *et al*, 1999). Two recent studies suggest a role for a DsbD-like protein in eukaryotes. The first study showed that depletion of glutathione did not affect folding of proteins requiring reductive disulfide shuffling (Tsunoda *et al*, 2014). The second study showed that reduction in non-native disulfides requires the cytosolic TRX system and postulated a role for a DsbD-like membrane protein to mediate electron transport to the ER (Poet *et al*, 2017). We found TRX and ERdj5, which could mimic bacterial TRX and DsbC, as LMF1-interacting proteins in our mass spectrometry results. Both were important for LPL, but not PL, secretion (Fig 2A and B). We found that LMF1 has conserved cysteines that contribute to LPL secretion (Fig 5C). It is thus tempting to speculate that LMF1 could function like DsbD.

Nonetheless, there are some key differences between LMF1 and DsbD. We could acid trap TRX and ERdj5 with LMF1, but these interactions were not especially robust, and complexes between the TRX trap and LMF1 were not captured (Fig 6). By contrast, DsbD-TRX and DsbD-DsbC trapping were robust and could be captured with the TRX trap (Katzen & Beckwith, 2000; Krupp *et al*, 2001). Oxidoreductases in the ER are known to be promiscuous, which likely explains the LMF1-TRX and LMF1-Erdj5 interactions that we saw (Oka *et al*, 2015). Additionally, we found eight cysteines in LMF1 needed for LPL secretion, but only five of these were completely conserved (Fig 5). By contrast, DsbD uses a set of six cysteines for its disulfide reduction cascade. Whereas DsbD has a canonical thioredoxin-like C-X-X-C motif for electron transfer, LMF1 does not have such a motif, which is needed for DsbD to function. Instead, there are two cysteines in LMF1's C-terminus, C445 and C453, which are separated by seven amino acids. Although not in a consensus C-X-X-C motif, these two cysteines are important. Specifically, of two naturally occurring truncation mutations in LMF1, one (Y439X) is positioned before C445 and one (W464X) is positioned after C453. The W464X variant retains about 30% of LPL secretion, whereas the Y439X variant does not detectably secrete LPL (Cefalu *et al*, 2009).

LMF1's extended family members suggest alternative mechanisms may exist for a transmembrane redox conduit. The Pfam database groups proteins into families based on sequence alignments and a profile hidden Markov model (HMM) analysis (Sonnhammer *et al*, 1998). Related families are grouped into clans, which have sequence, structure, or profile-HMM similarity (Finn *et al*, 2014). LMF1 belongs to a clan that includes the archaeal and bacterial transmembrane proteins DoxX, MauE, RclC, and DoxD, which are all involved in redox reactions. None are cysteine-rich. DoxX is a *Mycobacterium tuberculosis* multipass membrane protein that forms a complex with SodA and SseA to link detoxification of superoxide radicals generated during the phagocyte oxidative burst with cytosolic thiol homeostasis (Nambi

*et al*, 2015). MauE is a multipass membrane protein from *Paracoccus denitrificans*. MauE and its partner, MauD, are in an operon containing genes required for methylamine oxidation (van der Palen *et al*, 1997). MauD is a periplasmic protein with a thioredoxin-like fold that contains a CXXC motif. MauE and MauD are needed for proper folding of the  $\beta$ -subunit of methylamine dehydrogenase, a  $\beta$ -strand rich protein with six non-consecutive disulfide bonds (Huizinga *et al*, 1992; van der Palen *et al*, 1997). RclC is an *Escherichia coli* inner membrane protein with homology to quinone-binding proteins that are upregulated in response to reactive chlorine species (Parker *et al*, 2013). DoxD is a multipass membrane protein that, with its binding partner DoxA, oxidizes thiosulfate to reduce quinone (Muller *et al*, 2004). DoxDA can be purified as a quinone-binding complex from the membrane fraction of *Acidianus ambivalens* (Muller *et al*, 2004). Intriguingly, DoxDA is found in an operon with TrxP, a periplasmic reductase that can complement the loss of DsbC (Shouldice *et al*, 2010). The mechanisms by which DoxX, MauE, RclC, and DoxD carry out their functions are not yet understood.

Analysis of the DoxD, RclC, and DoxX domain architectures could also support a role for LMF1 in the fourth proposed mechanism for transferring reducing equivalents from the cytosol the ER: action of an unidentified, NADPH-dependent, ER-localized reductase (Ellgaard *et al*, 2018). In Pfam, DoxD, RclC, and DoxX domains are often fused to pyridine nucleotide-disulfide oxidoreductase domains (Finn *et al*, 2014). This domain family includes proteins with NADPH-binding domains such as thioredoxin reductase (Kuriyan *et al*, 1991). The ER contains the enzyme hexose-6-phosphate dehydrogenase (H6PD), which supplies NADPH to ER-resident reductases (Ozols, 1993). One such reductase, 11 $\beta$ -HSD1, acts on cortisone, but an enzyme that directly reduces PDIs in the ER is currently only hypothetical (Odermatt & Klusonova, 2015; Ellgaard *et al*, 2018). Loss of LMF1 resembles loss of H6PD in that the ER is more oxidized (Tsachaki *et al*, 2018). However, there is no evidence suggesting that LMF1 itself binds NADPH, but it could cooperate with such an enzyme.

Whereas there are open questions concerning the mechanism by which LMF1 contributes to ER redox homeostasis, the outcome of LMF1 activity is clear. We found that LDLR and fibronectin, both proteins with multiple disulfide bonds, are LMF1 substrates. It is thus likely that LMF1 has many additional substrates. We anticipate that other disulfide-rich proteins, in particular those that oligomerize, fold non-vectorially, and contain non-sequential disulfides, are likely to require LMF1 for efficient folding and secretion. In our hands, co-expression of LMF1 and LPL substantially enhances the amount of active, folded LPL secreted from cells. Increased LMF1 levels may thus enhance production or abundance of biologically or pharmaceutically important substrates such as LDLR.

## Materials and Methods

### Expression constructs

The construct for LMF1 with a C-terminal polyhistidine tag was previously described (Babilonia-Rosa & Neher, 2014). Site-directed mutagenesis of LMF1-His was employed to obtain C-to-A

mutations. Plasmids pSWAN-GFP37TAG and pSWAN-pBpaRS allowed for expression of suppressor tRNA and tRNA synthetase for incorporation of pBPA for photocrosslinking and were provided by P. Schultz (Liu *et al*, 2007). AvrII and BsrGI sites were used to remove GFP from the pSWAN-GFP37TAG and insert LMF1 with an 8X C-terminal polyhistidine tag. The amber codon was incorporated in the pSWAN-LMF1 in residue F262 using site-directed mutagenesis to generate pSWAN-Lmf1-F262Amber. For LPL-V5 and LPL-His, human LPL was excised from pCMV-SPORT6-LPL (Open Biosystems), a C-terminal V5 or His tag was added, and it was inserted into a pcDNA5/FRT vector (Thermo Fisher Scientific) using HindIII/BclI sites. To make the plasmid for expression of Txnip, the cDNA sequence of human Txnip was synthesized as a GBlock by IDT. It was digested using HindIII and XhoI and inserted in pcDNA5/FRT. Plasmids for expressing mCherry-Sec61 $\beta$  (#49155), YPet-tagged fibronectin (#65421), thioredoxin (#21614), and pSpCas9n-2A-Puro (#48141) were obtained from Addgene. Thioredoxin with a C35S mutation was generated using Quickchange. For CRISPR/Cas, plasmids pSN348 and pSN349 were generated from pGL3-U6-sgRNA-PGK- (Addgene plasmid #51133) by cutting with BsaI and inserting annealed oligo pairs 1 (ccgggaagactgggtactcggatc and aaacgatccgagtaccagcttc) and 2 (ccggcgcggcgccgccattgtt and aaacaacaatggcggcggcccg). The ERroGFP-S4 plasmid was a gift of Yasuyoshi Sakai group and Jun Hoseki at Kyoto University (Hoseki *et al*, 2016). The LDLR-GFP plasmid was a gift from Elizabeth Tarling at UCLA. A plasmid for expression of human ERdj5 with a V5 tag was obtained from the UNC Chapel Hill Lenti-cDNA Core facility (ORFeome clone # BC117299, RefSeq Gene NM\_018981.2).

### Cell lines and transfection

Stable HEK293 Flp-In™ (Thermo Scientific) cells lines were generated with LPL-V5, LPL-His, or LMF1-His as per manufacturer's direction. Specifically, Fugene 6 (Promega) was used as a transfection reagent and cells were selected with 200  $\mu$ g/ml of hygromycin. HEK293 cells were transiently transfected with Fugene 6 and 1  $\mu$ g of DNA for LMF1-His and the respective lipase construct for the DSP crosslinking experiment. *clt/clt* and *clt/wt* MEFs (Boedeker *et al*, 2001) were obtained from the Doolittle laboratory. Transfection of *clt/clt* cells on six-well plates was performed with 2  $\mu$ g of DNA and X-tremeGENE HP per manufacturer's instructions. All cell lines were maintained in Dulbecco's modified Eagle's medium with 10% fetal bovine serum, 1% penicillin/streptomycin, and 2 mM L-glutamine (complete media).

### CRISPR-Cas deletion of LMF1

CRISPR-Cas-mediated *LMF1* deletions were generated essentially as described (Shen *et al*, 2014). Briefly, HEK 293 Flp-In™ (Thermo Scientific) cells were transfected with 0.66  $\mu$ g each of pSpCas9n-2A-Puro, pSN348, and pSN349 using Fugene 6 (Promega). Cells were split into plates coated with fibronectin and selected with 2  $\mu$ g/ml of puromycin until untransfected cells died. Single colonies were selected, split into 96-well plates, and tested for their ability to secrete LPL. Genomic DNA was harvested from cells not secreting LPL, and the first exon of *LMF1* was amplified by PCR, cloned, and sequenced.

### siRNA knockdowns

siRNA transfections were performed with 20 nM of RNA oligonucleotide and 7  $\mu$ l of Lipofectamine RNAiMax (Life Technologies) per six-well plate, and samples were collected 48 h post-transfection. Validated Silencer Select siRNAs were obtained from Life Technologies: negative control No. 1 (4390843), ERp44 (s22965), PDI (s439), ERp72 (s18446), UGGT1 (132932), UGGT2 (112074), and ERdj5 (132773). Knockdown of protein expression was quantitated by Western blot using a ChemiDoc MP Imaging System from Bio-Rad and Image Lab Software. The percent of remaining protein expression was calculated with the following formula: ((Candidate/GAPDH)/(NC/GAPDH))\*100. Experiments were done in triplicate.

### Crosslinking and pull-down assays

For pull-down assays of LMF1-His from HEK Flp-In stable cell lines, two T-75 flasks per condition were seeded with  $7.5 \times 10^6$  cells. LMF1-His expression was induced with 2  $\mu$ g/ml tetracycline the next morning. The next day, cells were trypsinized, washed with 1 $\times$  PBS, crosslinked with 2 mM DSP (ProteoChem) with agitation for 30 min at room temperature, and quenched with 150 mM Tris pH 8. The cells were lysed by douncing in buffer 1 (250 mM NaCl, 10 mM Tris pH 8, and 1 mM PMSF). Following centrifugation for 20 min at 15,600  $\times$  g, pellets were resuspended by douncing with 1.4 ml of buffer 1. Lysates were incubated overnight with agitation and the addition of 20 mM fos-choline 12 (Anatrace). After centrifugation as above, 5% glycerol, 40 mM imidazole, and Ni-NTA agarose beads (Qiagen) were added to the supernatant. Beads were bound for 1 h at 4°C and then washed three times with 4 ml of buffer 2 (1 M NaCl, 10 mM Tris pH 8, 3 mM fos-choline 12.5% glycerol, 40 mM imidazole, and 1 mM PMSF) in 11 ml poly-prep chromatography columns (Bio-Rad). LMF1 complexes were eluted with buffer 3 (250 mM NaCl, 10 mM Tris pH 8, 3 mM fos-choline 12, 400 mM imidazole, and 1 mM PMSF). Eluate fractions were loaded on 8% SDS-PAGE, transferred to PVDF (Bio-Rad) for 75 min at 100 V, and blocked with 5% non-fat milk or BSA.

For photocrosslinking with pBpa, HEK293 cells were plated in six-well plates at  $10.5 \times 10^5$  cells per well; four wells were utilized per sample. The next day, 1  $\mu$ g of pSWAN-pBpaRS and pSWAN-Lmf1-F262Amber was transfected with Fugene 6. After 24 h, the media was replaced with media containing 2  $\mu$ g/ml of tetracycline, 0.5 mM pBpa (Chem-Impex International), and 0.3% of DMSO. Control wells lacked pBpa but contained 0.3% of DMSO. Cells were grown with pBPA for 24 h. The media was changed to 1 $\times$  PBS, and the cells were kept on ice and crosslinked with a UV lamp at a wavelength of 365 nm for 30 min at 2.5 cm from the lamp. LMF1 was purified from cells as described above.

### Lipase secretion

HEK293 $\Delta$ LMF1 were transfected with LMF1 C-to-A constructs 24 h before media collection. Three hours before media collection, lipase secretion was promoted by the addition of 600  $\mu$ l of DMEM with 1% FBS and 15 USP units/ml of heparin per 9.5 cm<sup>2</sup> well. The amount of lipase in media, soluble cell fraction and insoluble cell

fraction, was measured by Western blot. Cells were trypsinized and lysed with lysis buffer (150 mM NaCl, 1.0% Triton X-100, 50 mM Tris pH 8.0) and then separated by centrifugation. The soluble lysate fraction was removed, and the pellet fraction was solubilized with 5× SDS–PAGE sample buffer. Media, lysate, and pellet fractions were separated using 12% SDS–PAGE.

#### Analysis of LMF1 redox state

HEK293 + LMF1 cells were plated in a six-well plate at  $0.5 \times 10^6$  cells/ml. Cells were mock-transfected or transfected with 1 µg of the Txnip plasmid. LMF1-His expression was induced overnight with 2 µg/ml tetracycline, and the next morning, cells were precipitated with ice-cold, 8% TCA, washed with acetone, and resuspended with an automated homogenizer in 50 mM Tris pH 8, 4% SDS with or without 10 mM AMS. Prior to precipitation, cells were either untreated or treated with 1 mM H<sub>2</sub>O<sub>2</sub> for 30 min or 10 mM DTT for 10 min. Samples were separated on 12% SDS–PAGE for 3 h at 180 V and then analyzed by Western blot as described below.

#### Analysis of LMF1 and ERdj5 or Trx interaction

HEK293 + LMF1 cells or HEK293ΔLMF1 were plated in a T75 flask at a density of  $5 \times 10^6$  cells 48 h prior to use. Each flask was transfected with 12 µg of either mCherry (control), ERdj5-V5, or Trx-C35S plasmid 24 h before harvesting. Expression was induced with tetracycline at the time of transfection. At harvesting, cells were washed with cold 10 mM NEM in PBS, trypsinized, and pelleted. Cells were resuspended in PBS and TCA precipitated with 8% TCA on ice for 30 min and pelleted at  $13,000 \times g$  at 4°C for 10 min. Pellets were resuspended in denaturing alkylating buffer (6 M urea, 1% SDS, 100 mM Tris pH 7.5) plus 50 mM NEM. Lysates were diluted 1:10 in Triton buffer (2% Triton-X100, 50 mM Tris pH 7, 150 mM NaCl, 6 M urea) plus 20 mM NEM. Fos-choline 12 was added to 3 mM, and resuspended lysates were incubated overnight at 4°C. Lysates were cleared by centrifugation at  $13,000 \times g$  for 5 min at 4°C. Cleared lysates were batch bound to 150 µl of Ni-NTA Excel (GE Healthcare) resin for 2 h at 4°C. Beads were washed 4 × with 3 ml of Triton buffer plus 10 mM imidazole and then eluted 2 × 150 µl with Triton buffer plus 500 mM imidazole. Eluted samples were incubated with 2.5 M urea in 2× SDS loading dye with or without 50 mM DTT for 10 min at room temperature and then heated to 72°C for 4 min before resolution by SDS–PAGE. Westerns were performed as described below.

#### Antibodies and Western blots

For Western blots, samples mixed with 5× SDS loading dye (0.2 M Tris pH 8.0, 1% SDS, 30% glycerol, ±40 mM DTT) and separated using SDS–PAGE. Proteins were then transferred to PVDF using a wet transfer (Bio-Rad). Blots were blocked for 2 h. Blots were then incubated with antibodies at dilutions listed below for 1 h at room temperature. Blots were washed three times in TBST for 10 min each. Blots were incubated with anti-rabbit or anti-mouse HRP secondary antibody at 1:20,000 in 2.5% milk/TBST for 45 min and then washed three times in TBST. Blots were incubated with ECL substrate (ADVANTA WesternBright, BioExpress) and

proteins detected with a ChemiDoc MP Imaging System from Bio-Rad and Image Lab Software. For Western blots of LPL and PL aggregates, gels were soaked in 10 mM DTT for 10 min prior to transfer.

LMF1-His was detected with an anti-His antibody (1:5,000 AbD Serotec). PDI, ERp72, and ERp44 antibodies were obtained from Cell Signaling, used at 1:1,000 in 5% BSA, and with HRP-conjugated anti-rabbit (Southern Biotech) at 1:5,000. UGGT1, UGGT2, ERdj5, TRX, and TXNIP antibodies were obtained Abcam; used at 1:500, 1:1,000, 1:500, 1:1,000, and 1:600, respectively, in 5% BSA with HRP-conjugated anti-mouse or anti-rabbit antibodies from Southern Biotech. Mouse anti-V5 antibody from Bio-Rad was diluted 1:5,000 in 5% non-fat milk in TBST. The c-Myc antibody (MA1980, Invitrogen) was used at a dilution of 1:1,000 in 5% non-fat milk in TBST.

#### Translation and protein-folding assays

Assays were based on previously described methods (Francis *et al*, 2002; Poet *et al*, 2017). To generate mRNA, the pCMV-SPORT6-LPL template plasmid was linearized with HindIII. RNA was transcribed using the mMessage mMachine SP6 Transcription kit (Invitrogen) per the manufacturer's directions. To generate SP cells, HEK293 or HEK293ΔLMF1 was grown to 70% confluence, trypsinized, pelleted, and resuspended in KHM buffer (110 mM KOAc, 2 mM MgOAc, 20 mM HEPES pH 7.2) with Digitonin (20 µg/ml) and then incubated for 8 min on ice. Cells were pelleted at  $100 \times g$  for 4 min at 4°C and resuspended in potassium acetate/HEPES buffer (90 mM HEPES pH 7.2, 50 mM KOAc pH 7.2) and incubated for 10 min on ice. Cells were pelleted again at  $100 \times g$  for 4 min at 4°C and resuspended in micrococcal nuclease buffer (KHM supplemented with 1.5 mM CaCl<sub>2</sub>) with micrococcal nuclease (NEB) added for 12 min at room temperature. Digestion was arrested with 4 mM EGTA, and cells were pelleted at  $100 \times g$  for 4 min at 4°C, washed with KHM buffer, and resuspended in 50 µl KHM buffer. Cells were counted and used immediately.

Metabolic labeling and pulse-chase analysis: Translation mix was prepared using the Flexi rabbit reticulocyte lysate (Promega) with the following components added to a final volume of 25 µl: 16.5 µl lysate, KCl at 70 mM, amino acid mixture minus methionine at 200 µM, RNasin (Promega) at 40 U/µl, 750 ng RNA,  $8.8 \times 10^4$  SP cells, 11 µCi of EasyTag™ EXPRESS<sup>35</sup>S mix (PerkinElmer), and nuclease-free water. Mixtures were incubated at 30°C for 1 h, and then, 1 mM cycloheximide (Sigma) was added to stop translation. At the indicated time points, 15 µl of reaction mix was removed and added to either SDS loading dye and put on ice or 14 mM AMS (Invitrogen) and incubated for 1 h in the dark. 1× SDS loading dye was added to all samples and boiled for 3 min at 80°C. Samples were spun down, and lysates of equal volumes were separated by SDS–PAGE. SDS Gels were dried, exposed, and imaged on a Typhoon FLA 9500 (GE), and quantification was carried out in Fiji.

#### Mass spectrometry

Gel slices containing purified LMF1 with pBPA- or DSP cross-linked-binding partners were analyzed by the Duke proteomic facility. Control gel slices were obtained from samples prepared

without pBpa (pBpa experiment) or without tetracycline for induction (DSP). Coomassie-stained SDS-PAGE bands were subjected to standardized in-gel trypsin digestion. Extracted peptides were lyophilized to dryness and resuspended in 12  $\mu$ l of 0.2% formic acid/2% acetonitrile. Each sample was subjected to chromatographic separation on a Waters NanoAcquity UPLC equipped with a 1.7  $\mu$ m BEH130 C<sub>18</sub> 75  $\mu$ m I.D. X 250 mm reversed-phase column. The mobile phase consisted of (A) 0.1% formic acid in water, and (B) 0.1% formic acid in acetonitrile. Following a 3  $\mu$ l injection, peptides were trapped for 3 min on a 5  $\mu$ m Symmetry C<sub>18</sub> 180  $\mu$ m I.D. X 20 mm column at 5  $\mu$ l/min in 99.9% A. The analytical column was then switched in-line, and a linear elution gradient of 5% B to 40% B was performed over 30 min at 400 nl/min. The analytical column was connected to a fused silica PicoTip emitter (New Objective, Cambridge, MA) with a 10- $\mu$ m tip orifice and coupled to a Q Exactive Plus mass spectrometer (Thermo Scientific) through an electrospray interface operating in a data-dependent mode of acquisition. The instrument was set to acquire a precursor MS scan from *m/z* 375–1,675 with MS/MS spectra acquired for the 10 most abundant precursor ions. For all experiments, HCD energy settings were 27v and a 120 s dynamic exclusion was employed for previously fragmented precursor ions.

Raw LC-MS/MS data files were processed in Proteome Discoverer (Thermo Scientific) and then submitted to independent Mascot searches (Matrix Science) against a SwissProt database (*Human* taxonomy) containing both forward and reverse entries of each protein (20,322 forward entries). Search tolerances were 5 ppm for precursor ions and 0.02 Da for product ions using trypsin specificity with up to two missed cleavages. Carbamidomethylation (+57.0214 Da on C) was set as a fixed modification, whereas oxidation (+15.9949 Da on M) and deamidation (+0.98 Da on NQ) were considered dynamic mass modifications. All searched spectra were imported into Scaffold (v4.3, Proteome Software), and scoring thresholds were set to achieve a peptide false discovery rate of 1% using the PeptideProphet algorithm. The mass spectrometry proteomics data have been deposited to the ProteomeXchange Consortium via the PRIDE partner repository with the dataset identifier PXD009641 (<https://doi.org/10.6019/PXD009641>).

### BSO, DTT, and tunicamycin sensitivity

To assess cell sensitivity to BSO, DTT, and tunicamycin, first  $1 \times 10^5$  cells/well of *cld/cld* or *cld/wt* were plated in a six-well plate. The next day, either vehicle control, 10 mM L-BSO, 2.5  $\mu$ g/ml tunicamycin, or 5 mM DTT was added. After 24 (tunicamycin or BSO) or 12 (DTT) hours of treatment, cells were removed from the plate with trypsin, stained with trypan blue, and live cells were manually counted using a hemocytometer. For HEK293/HEK293 $\Delta$ LMF1 cells, cells were plated in six-well plates coated with fibronectin (Invitrogen). Cells were treated with 2  $\mu$ g/ml Tunicamycin for 20 h, with 10 mM L-BSO for 24 h or 10 mM DTT for 12 h. Cells were trypsinized, stained, and live cells were counted on a Countess II cell counter (Invitrogen). For both cell types, survival was reported relative to vehicle control. Three wells were counted for each condition and the average survival was calculated, and three of these independent experiments were carried out per condition.

### Live cell imaging

For all experiments, cells were plated in poly-d-lysine coated 33-mm glass bottom Petri dishes, with 14 mm microwell, No. 1.5 cover glass (MatTek). For characterization of fibronectin in HEK293, HEK293 $\Delta$ LMF1, *cld/wt*, and *cld/cld* cells,  $1.3 \times 10^5$  cells were transfected with X-tremeGENE (Roche) with 1.2  $\mu$ g plasmid expressing fibronectin-YPet and mCherry-Sec61 $\beta$ . The transfection media was removed 6–7 h post-transfection, and the cells were washed with PBS and then returned to culture media. Images were taken 24 h post-transfection at 37°C in a CO<sub>2</sub> chamber with a Zeiss LSM 710 confocal microscope and a Plan Apo 40 $\times$ /1.4 NA oil objective. For quantification, the images were first deconvolved using the AutoQuant 3D Deconvolution function. A threshold for each probe was then determined using the Threshold Plugin of Fiji. Using these thresholds, colocalization percentages were calculated using Imaparis (Bitplane).

For characterization of the redox environment in cells, HEK293 or HEK293 $\Delta$ LMF1 cells were transfected with 1  $\mu$ g ERroGFP-S4 plasmid and in some experiments 0.4  $\mu$ g LPL-mCherry plasmid with Fugene HD (Promega) 24 h prior to imaging. Cells were imaged on a Zeiss LSM 710 laser scanning microscope as described above. All images were taken at identical gain, offset, and laser intensities between groups. To assess cellular redox state, ERroGFP was excited by 405 and 458 nm lasers and emission was collected between 504 and 533 nm in independent frames. Background intensity was subtracted automatically with Fiji, and three random ROIs were drawn on each cell body and mean intensity was measured in Fiji. The mean intensity of tracks 405 to 458 were compared to generate a ratio describing the oxidized GFP state (405 nm) to reduced GFP state (458). For each of three independent experiments, three spots from 17 cells were imaged. Representative data are shown.

**Expanded View** for this article is available online.

### Acknowledgements

We thank Deb Muoio for advice about Txnip, Eric Brustad for advice on use of pBPA, Pablo Ariel for assistance with microscopy, and Stephanie Gupton, Edward Bahnon, Ciara Gallagher, Doug Cyr, and members of the Neher and Campbell laboratories for advice on the manuscript. This work was supported by NHLBI Grant R00HL098277 and AHA grant 17GRNT33700219 to SBN. MAB was supported by a UNC Dissertation Completion Fellowship. BSR is supported by grant 2T32HL069768.

### Author contributions

MAB-R, BSR, LJB, SBN, and MJW designed and carried out experiments. SBN, MAB-R, and BSR prepared figures. SBN wrote the manuscript.

### Conflict of interest

The authors declare that they have no conflict of interest.

### References

- Arnold SM, Fessler LI, Fessler JH, Kaufman RJ (2000) Two homologues encoding human UDP-glucose:glycoprotein glucosyltransferase differ in mRNA expression and enzymatic activity. *Biochemistry* 39: 2149–2163

- Babilonia-Rosa M, Neher SB (2014) Purification, cellular levels, and functional domains of LMF1. *Biochem Biophys Res Commun* 450: 423–428
- Ben-Zeev O, Mao HZ, Doolittle MH (2002) Maturation of lipoprotein lipase in the endoplasmic reticulum. Concurrent formation of functional dimers and inactive aggregates. *J Biol Chem* 277: 10727–10738
- Ben-Zeev O, Hosseini M, Lai CM, Ehrhardt N, Wong H, Cefalu AB, Noto D, Aversa MR, Doolittle MH, Peterfy M (2011) Lipase maturation factor 1 is required for endothelial lipase activity. *J Lipid Res* 52: 1162–1169
- Berkmen M, Boyd D, Beckwith J (2005) The nonconsecutive disulfide bond of *Escherichia coli* phytase (AppA) renders it dependent on the protein-disulfide isomerase, DsbC. *J Biol Chem* 280: 11387–11394
- Boedeker JC, Doolittle MH, White AL (2001) Differential effect of combined lipase deficiency (cld/cld) on human hepatic lipase and lipoprotein lipase secretion. *J Lipid Res* 42: 1858–1864
- Briquet-Laugier V, Ben-Zeev O, White A, Doolittle MH (1999) cld and lec23 are disparate mutations that affect maturation of lipoprotein lipase in the endoplasmic reticulum. *J Lipid Res* 40: 2044–2058
- Cefalu AB, Noto D, Arpi ML, Yin F, Spina R, Hilden H, Barbagallo CM, Carroccio A, Tarugi P, Squatrito S, Vigneri R, Taskinen MR, Peterfy M, Aversa MR (2009) Novel LMF1 nonsense mutation in a patient with severe hypertriglyceridemia. *J Clin Endocrinol Metab* 94: 4584–4590
- Davis RC, Ben-Zeev O, Martin D, Doolittle MH (1990) Combined lipase deficiency in the mouse. Evidence of impaired lipase processing and secretion. *J Biol Chem* 265: 17960–17966
- Doolittle MH, Neher SB, Ben-Zeev O, Ling-Liao J, Gallagher CM, Hosseini M, Yin F, Wong H, Walter P, Peterfy M (2009) Lipase maturation factor LMF1, membrane topology and interaction with lipase proteins in the endoplasmic reticulum. *J Biol Chem* 284: 33623–33633
- Elgaard L, Sevier CS, Bulleid NJ (2018) How are proteins reduced in the endoplasmic reticulum? *Trends Biochem Sci* 43: 32–43
- Finn RD, Bateman A, Clements J, Coghill P, Eberhardt RY, Eddy SR, Heeger A, Hetherington K, Holm L, Mistry J, Sonnhammer EL, Tate J, Punta M (2014) Pfam: the protein families database. *Nucleic Acids Res* 42: D222–D230
- Francis E, Daniels R, Hebert DN (2002) Analysis of protein folding and oxidation in the endoplasmic reticulum. *Curr Protoc Cell Biol Chapter* 15, Unit 15 16
- Hampe L, Radjainia M, Xu C, Harris PW, Bashiri G, Goldstone DC, Brimble MA, Wang Y, Mitra AK (2015) Regulation and quality control of adiponectin assembly by endoplasmic reticulum chaperone ERp44. *J Biol Chem* 290: 18111–18123
- Hegele RA, Pollex RL (2009) Hypertriglyceridemia: phenomics and genomics. *Mol Cell Biochem* 326: 35–43
- Hoseki J, Oishi A, Fujimura T, Sakai Y (2016) Development of a stable ERroGFP variant suitable for monitoring redox dynamics in the ER. *Biosci Rep* 36: e00316
- Huizinga EG, van Zanten BA, Duine JA, Jongejan JA, Huitema F, Wilson KS, Hol WG (1992) Active site structure of methylamine dehydrogenase: hydrazines identify C6 as the reactive site of the tryptophan-derived quinone cofactor. *Biochemistry* 31: 9789–9795
- Jansens A, van Duijn E, Braakman I (2002) Coordinated nonvectorial folding in a newly synthesized multidomain protein. *Science* 298: 2401–2403
- Jessop CE, Tavender TJ, Watkins RH, Chambers JE, Bulleid NJ (2009a) Substrate specificity of the oxidoreductase ERp57 is determined primarily by its interaction with calnexin and calreticulin. *J Biol Chem* 284: 2194–2202
- Jessop CE, Watkins RH, Simmons JJ, Tasab M, Bulleid NJ (2009b) Protein disulphide isomerase family members show distinct substrate specificity: P5 is targeted to BiP client proteins. *J Cell Sci* 122: 4287–4295
- Katzen F, Beckwith J (2000) Transmembrane electron transfer by the membrane protein DsbD occurs via a disulfide bond cascade. *Cell* 103: 769–779
- Ko MK, Kay EP (2004) PDI-mediated ER retention and proteasomal degradation of procollagen I in corneal endothelial cells. *Exp Cell Res* 295: 25–35
- Krupp R, Chan C, Missiakas D (2001) DsbD-catalyzed transport of electrons across the membrane of *Escherichia coli*. *J Biol Chem* 276: 3696–3701
- Kuriyan J, Krishna TS, Wong L, Guenther B, Pahler A, Williams CH Jr, Model P (1991) Convergent evolution of similar function in two structurally divergent enzymes. *Nature* 352: 172–174
- Liu W, Brock A, Chen S, Schultz PG (2007) Genetic incorporation of unnatural amino acids into proteins in mammalian cells. *Nat Methods* 4: 239–244
- Maegawa KI, Watanabe S, Noi K, Okumura M, Amagai Y, Inoue M, Ushioda R, Nagata K, Ogura T, Inaba K (2017) The highly dynamic nature of ERdj5 is key to efficient elimination of aberrant protein oligomers through ER-associated degradation. *Structure* 25: 846–857 e4
- Meister A (1983) Selective modification of glutathione metabolism. *Science* 220: 472–477
- Muller FH, Bandejas TM, Urich T, Teixeira M, Gomes CM, Kletzin A (2004) Coupling of the pathway of sulphur oxidation to dioxygen reduction: characterization of a novel membrane-bound thiosulphate: quinone oxidoreductase. *Mol Microbiol* 53: 1147–1160
- Nambi S, Long JE, Mishra BB, Baker R, Murphy KC, Olive AJ, Nguyen HP, Shaffer SA, Sasseti CM (2015) The oxidative stress network of *Mycobacterium tuberculosis* reveals coordination between radical detoxification systems. *Cell Host Microbe* 17: 829–837
- Odermatt A, Klusonova P (2015) 11beta-Hydroxysteroid dehydrogenase 1: Regeneration of active glucocorticoids is only part of the story. *J Steroid Biochem Mol Biol* 151: 85–92
- Oka OB, Pringle MA, Schopp IM, Braakman I, Bulleid NJ (2013) ERdj5 is the ER reductase that catalyzes the removal of non-native disulfides and correct folding of the LDL receptor. *Mol Cell* 50: 793–804
- Oka OB, Yeoh HY, Bulleid NJ (2015) Thiol-disulfide exchange between the PDI family of oxidoreductases negates the requirement for an oxidase or reductase for each enzyme. *Biochem J* 469: 279–288
- Ozols J (1993) Isolation and the complete amino acid sequence of luminal endoplasmic reticulum glucose-6-phosphate dehydrogenase. *Proc Natl Acad Sci USA* 90: 5302–5306
- van der Palen CJ, Reijnders WN, de Vries S, Duine JA, van Spanning RJ (1997) MauE and MauD proteins are essential in methylamine metabolism of *Paracoccus denitrificans*. *Antonie Van Leeuwenhoek* 72: 219–228
- Parker BW, Schwessinger EA, Jakob U, Gray MJ (2013) The RclR protein is a reactive chlorine-specific transcription factor in *Escherichia coli*. *J Biol Chem* 288: 32574–32584
- Paterniti JR Jr, Brown WV, Ginsberg HN, Artzt K (1983) Combined lipase deficiency (cld): a lethal mutation on chromosome 17 of the mouse. *Science* 221: 167–169
- Patwari P, Higgins LJ, Chutkow WA, Yoshioka J, Lee RT (2006) The interaction of thioredoxin with Txnip. Evidence for formation of a mixed disulfide by disulfide exchange. *J Biol Chem* 281: 21884–21891
- Peterfy M, Ben-Zeev O, Mao HZ, Weissglas-Volkov D, Aouizerat BE, Pullinger CR, Frost PH, Kane JP, Malloy MJ, Reue K, Pajukanta P, Doolittle MH (2007) Mutations in LMF1 cause combined lipase deficiency and severe hypertriglyceridemia. *Nat Genet* 39: 1483–1487



- Poet GJ, Oka OB, van Lith M, Cao Z, Robinson PJ, Pringle MA, Arner ES, Bulleid NJ (2017) Cytosolic thioredoxin reductase 1 is required for correct disulfide formation in the ER. *EMBO J* 36: 693–702
- Ponsero AJ, Igbaria A, Darch MA, Miled S, Outten CE, Winther JR, Palais G, D'Autreaux B, Delaunay-Moisan A, Toledano MB (2017) Endoplasmic reticulum transport of glutathione by Sec61 is regulated by Ero1 and Bip. *Mol Cell* 67: 962–973 e965
- Rietsch A, Bessette P, Georgiou G, Beckwith J (1997) Reduction of the periplasmic disulfide bond isomerase, DsbC, occurs by passage of electrons from cytoplasmic thioredoxin. *J Bacteriol* 179: 6602–6608
- Rutkevich LA, Cohen-Doyle MF, Brockmeier U, Williams DB (2010) Functional relationship between protein disulfide isomerase family members during the oxidative folding of human secretory proteins. *Mol Biol Cell* 21: 3093–3105
- Searle BC (2010) Scaffold: a bioinformatic tool for validating MS/MS-based proteomic studies. *Proteomics* 10: 1265–1269
- Sha H, Sun S, Francisco AB, Ehrhardt N, Xue Z, Liu L, Lawrence P, Mattijssen F, Guber RD, Panhwar MS, Brenna JT, Shi H, Xue B, Kersten S, Bensadoun A, Peterfy M, Long Q, Qi L (2014) The ER-associated degradation adaptor protein Sel1L regulates LPL secretion and lipid metabolism. *Cell Metab* 20: 458–470
- Shen B, Zhang W, Zhang J, Zhou J, Wang J, Chen L, Wang L, Hodgkins A, Iyer V, Huang X, Skarnes WC (2014) Efficient genome modification by CRISPR-Cas9 nickase with minimal off-target effects. *Nat Methods* 11: 399–402
- Shouldice SR, Cho SH, Boyd D, Heras B, Eser M, Beckwith J, Riggs P, Martin JL, Berkmen M (2010) *In vivo* oxidative protein folding can be facilitated by oxidation-reduction cycling. *Mol Microbiol* 75: 13–28
- Sievers F, Wilm A, Dineen D, Gibson TJ, Karplus K, Li W, Lopez R, McWilliam H, Remmert M, Soding J, Thompson JD, Higgins DG (2011) Fast, scalable generation of high-quality protein multiple sequence alignments using Clustal Omega. *Mol Syst Biol* 7: 539
- Sonnhammer EL, Eddy SR, Birney E, Bateman A, Durbin R (1998) Pfam: multiple sequence alignments and HMM-profiles of protein domains. *Nucleic Acids Res* 26: 320–322
- Stewart EJ, Katzen F, Beckwith J (1999) Six conserved cysteines of the membrane protein DsbD are required for the transfer of electrons from the cytoplasm to the periplasm of *Escherichia coli*. *EMBO J* 18: 5963–5971
- Tsachaki M, Mladenovic N, Stamberгова H, Birk J, Odermatt A (2018) Hexose-6-phosphate dehydrogenase controls cancer cell proliferation and migration through pleiotropic effects on the unfolded-protein response, calcium homeostasis, and redox balance. *FASEB J* 32: 2690–2705
- Tsunoda S, Avezov E, Zyryanova A, Konno T, Mendes-Silva L, Pinho Melo E, Harding HP, Ron D (2014) Intact protein folding in the glutathione-depleted endoplasmic reticulum implicates alternative protein thiol reductants. *Elife* 3: e03421
- Ushioda R, Hoseki J, Araki K, Jansen G, Thomas DY, Nagata K (2008) ERdj5 is required as a disulfide reductase for degradation of misfolded proteins in the ER. *Science* 321: 569–572
- Vartio T, Kuusela P (1991) Disulfide-bonded dimerization of fibronectin *in vitro*. *Eur J Biochem* 202: 597–604
- Zhang L, Wu G, Tate CG, Lookene A, Olivecrona G (2003) Calreticulin promotes folding/dimerization of human lipoprotein lipase expressed in insect cells (sf21). *J Biol Chem* 278: 29344–29351